CrossMark

Investigating the [C II]-to-H I Conversion Factor and the H I Gas Budget of Galaxies at $z \approx 6$ with Hydrodynamic Simulations

David Vizgan[1,2,3] , Kasper E. Heintz[1,4] , Thomas R. Greve[1,2,5] , Desika Narayanan[1,6] , Romeel Davé[7,8] ,
Karen P. Olsen[9] , Gergö Popping[10] , and Darach Watson[1,4]

[1] The Cosmic Dawn Center
[2] National Space Institute, DTU Space, Technical University of Denmark, DK-2800 Kgs. Lyngby, Denmark
[3] Department of Astronomy, University of Illinois at Urbana-Champaign, 1002 West Green St., Urbana, IL 61801, USA
[4] Niels Bohr Institute, University of Copenhagen, Lyngbyvej 2, DK-2100 Copenhagen, Denmark
[5] Department of Physics and Astronomy, University College London, Gower Place, WC1E 6BT London, UK
[6] Department of Astronomy, University of Florida, Gainesville, FL 32611, USA
[7] Institute for Astronomy, University of Edinburgh, Edinburgh EH9 3HJ, UK
[8] University of the Western Cape, Bellville, Cape Town 7535, South Africa
[9] Department of Astronomy and Steward Observatory, University of Arizona, Tucson, AZ 85721, USA
[10] European Southern Observatory, D-85478 Garching bei München, Germany
Received 2022 June 27; revised 2022 October 7; accepted 2022 October 7; published 2022 October 26

Abstract

One of the most fundamental baryonic matter components of galaxies is the neutral atomic hydrogen (H I). At low redshifts, this component can be traced directly through the 21 cm transition, but to infer the H I gas content of the most distant galaxies, a viable tracer is needed. We here investigate the fidelity of the fine-structure transition of the $(^2P_{3/2} - ^2P_{1/3})$ transition of singly ionized carbon C II at 158 μm as a proxy for H I in a set simulated galaxies at $z \approx 6$, following the work by Heintz et al. We select 11,125 star-forming galaxies from the SIMBA simulations, with far-infrared line emissions postprocessed and modeled within the SIGAME framework. We find a strong connection between C II and H I, with the relation between this C II-to-H I relation ($\beta_{[C \, II]}$) being anticorrelated with the gas-phase metallicity of the simulated galaxies. We further use these simulations to make predictions for the total baryonic matter content of galaxies at $z \approx 6$, and specifically the H I gas mass fraction. We find mean values of $M_{H \, I}/M_\star = 1.4$ and $M_{H \, I}/M_{bar,tot} = 0.45$. These results provide strong evidence for H I being the dominant baryonic matter component by mass in galaxies at $z \approx 6$.

Unified Astronomy Thesaurus concepts: High-redshift galaxies (734); Astronomical simulations (1857); Interstellar medium (847); Interstellar atomic gas (833)

1. Introduction

In the process of galaxy formation, the infall of neutral atomic hydrogen (H I) is a necessary, fundamental ingredient in the formation of stars. Reservoirs of H I gas condense into molecular hydrogen (H_2), which serves as fuel for star formation. As such, H I is a crucial component for the assembly of galaxies and thus governs the first epoch of galaxy formation. At higher redshifts ($z > 3$) H I can also reveal large-scale structure of the universe by tracing the precursors to superclusters of galaxies (e.g., Scott & Rees 1990).

The main tracer of H I is the $\lambda = 21$ cm line, which arises from transitions between the hyperfine structure levels in the ground state of the hydrogen atom. There are many benefits, in theory, of utilizing the 21 cm line; for instance, it does not suffer from dust extinction and attenuation like other lines, and kinematic information about the emitting gas can be derived from its Doppler shift (Walter et al. 2008). Even though H I has been observed within our own Galaxy (e.g., Kalberla et al. 2005) and for many galaxies locally (e.g., Thuan & Martin 1981; Swaters et al. 2002; Walter et al. 2008), few detections of the 21 cm line emission have been made beyond $z \approx 0.3$ (Bera et al. 2019), mainly due to the weakness of the transition and the limited sensitivity (Carilli & Walter 2013). The current most

distant estimate for a single galaxy has reached $z = 0.376$ (Fernandez et al. 2016), with other recent works examining the average 21 cm signal from a stack of a few thousand galaxies out to $z \approx 1$ (Chowdhury et al. 2020, 2021). Although the evolution of the H I budget across redshift has been modeled via theoretical predictions (Madau & Dickinson 2014), our understanding of the fueling of star formation rate across cosmic time is incomplete without an understanding of how the contribution of H I to the total composition of galaxies evolves with redshift, from the epoch of reionization until today.

To infer the H I gas content of even more distant galaxies, it is clear that a suitable tracer has to be identified as a proxy. This is similar to how observations of in particular CO and [C I] has been used as tracers of the molecular gas content of galaxies through most of cosmic time (e.g., Papadopoulos & Greve 2004; Bolatto et al. 2013). We here investigate the 158 μm (1900.5 GHz) fine-structure transition of singly ionized carbon ([CII]) as a potential tracer of H I. This particular transition was suggested by Morton & Hu (1975) early on to be a strong cooling line within H I regions. Further work by Tielens & Hollenbach (1985), Wolfire et al. (1995), Hollenbach & Tielens (1999), and Wolfire et al. (2003) chemically examined the role of C II in the cooling of photodissociation regions (PDRs) and the cold and warm neutral medium (CNM and WNM, respectively). Observationally, Madden et al. (1993) found that extended C II emission in NGC 6946 likely emerged from cold, atomic hydrogen clouds. Madden et al. (1997) investigated a correlation between C II luminosity and the H I gas mass ($M_{H \, I}$) in the local irregular galaxy IC 10, finding

that while most C II emission arose from dense PDRs, ~20% of the emission could arise from atomic hydrogen regions in the interstellar medium (ISM) of the galaxy. More recent work relying on hydrodynamic simulations of galaxies (e.g., Vallini et al. 2015; Lupi & Bovino 2020; Ramos Padilla et al. 2021, 2022) has constrained the fraction of C II originating from different ISM phases, showing that it is more predominantly produced in neutral H I regions at higher redshifts. As C II is one of the strongest cooling lines in the ISM, it is one of the brightest far-infrared lines and thus easily observable at high redshifts (Stacey et al. 2010). This makes it a natural candidate as a potential proxy for H I at $z \approx 6$. With the further evidence to support it as a tracer of H I in the local universe, and the strong connection found in high-redshift gamma-ray burst (GRB) sightlines (Heintz et al. 2021), we here wish to further explore the feasibility of C II as a tracer of H I based on simulations to (a) clarify and further investigate the viability of C II as a proxy for H I, (b) make predictions for the H I gas mass fraction in galaxies at $z \approx 6$, and (c) examine the underlying physics that drive this correlation.

The paper is structured as follows: In Section 2 we describe the observational and hydrodynamic simulation samples utilized for the purposes of this work. In Section 3 we describe the C II–HI relation both in equation form and in terms of a single conversion factor, $\beta_{[C\ II]}$, and analyze the effect of metallicity on $\beta_{[C\ II]}$. In Section 4 we investigate the H I budget at $z \approx 6$. We conclude this work in Section 5.

2. Simulations and Observational Samples

This work uses a set of SIMBA (Dave et al. 2019) galaxy simulations at $z = 5.93$, with line emission simulated and postprocessed using v2 of SIGAME (Olsen et al. 2017). The SIMBA simulation set consists of three cubical volumes of 25, 50, and 100 cMpc h^{-1} on a side, all of which are used in this work to search for galaxies at $z \sim 6$. For each volume, a total of 1024^3 gas elements and 1024^3 dark matter particles are evolved from $z = 249$.

Within these three volumes, a total of 11,137 galaxies were selected via the YT (Turk et al. 2011)-based package CAESAR; YT is a Python package used to visualize and analyze volumetric data, and CAESAR is a six-dimensional friends-of-friends algorithm that is applied to the simulated gas and stellar particles to identify and select SIMBA galaxies. The galaxy properties derived with CAESAR include star formation rate (SFR), computed by dividing the stellar mass formed over a 100 Myr timescale (Leung et al. 2020), SFR surface density, stellar mass ($M_\star$), and an SFR-weighted gas-phase metallicity (Z). The ionized, molecular, and atomic gas masses are calculated via CAESAR to be equal to the total mass of all gas particles associated with each respective phase (we refer to Olsen et al. 2017; Vizgan et al. 2022, for further description of how these gas "particles" are defined and constructed).

Our final sample consists of 11,125 galaxies, with C II luminosities in the range $L_{[C\ II]} = 10^{3.82} - 10^{8.91}\ L_\odot$ and molecular gas masses $M_{mol} = 10^{6.25} - 10^{10.33}\ M_\odot$, with a mean $M_\star$ of $10^{8.07}\ M_\odot$, mean SFR of 1.9 $M_\odot$ yr^{-1}, and mean metallicity of 0.18 $Z_\odot$. We refer to Leung et al. (2020) and Vizgan et al. (2022) for further description and detailing of SIMBA, SIGAME, CAESAR, and the simulation sample.

In this work, we define the total H I gas mass in each galaxy to be equal to the sum of its ionized and atomic hydrogen gas mass, independent of galactic region or radius. Molecular clouds have been shown observationally to also consist of a substantial fraction of H I and will thereby also contribute to the

total H I gas mass. The fraction of H I in molecular clouds has been measured to vary between 20% and 80% in our Galaxy (Burgh et al. 2010), so here we assume that ~50% of the total molecular gas in our simulations is H I. Similarly, a significant H I volume filling fraction of ≈50% has been derived for interstellar H I within the warm neutral medium in the solar neighborhood (Heiles & Troland 2003). The way that SIGAME classifies gas particles as "ionized" in this gas phase is by requiring that its electron-to-hydrogen fraction is $x_{e^-} > 0.5$; consequently, a gas particle in SIGAME will be considered completely ionized beyond $x_{e^-} > 0.5$, and otherwise neutral. This is not realistic when considering a real galaxy and we thus assume ~50% of the ionized gas will contribute to the atomic gas mass because of this classification. Because of this assumption, the gas masses derived from simulations should technically be treated as upper limits on the neutral gas budget.

We supplement our simulation sets with some observational samples of C II observations from the literature. We use H I gas masses (Cormier et al. 2015) of main-sequence dwarf galaxies with C II observations in the local Herschel Dwarf Galaxy Survey (Madden et al. 2013), which serve as high-redshift analogs. In addition, we use the X-shooter GRB afterglow legacy sample (XS-GRB; Selsing et al. 2019), which covers a redshift range between 0.059 and 7.84 and which was detected with the Swift satellite. Metallicities and H I column densities of these GRBs are taken from Bolmer et al. (2019), and the C II column densities are taken from Heintz et al. (2021).

3. The [C II]-to-[H I] Relation

3.1. Connecting $L_{[CII]}$ and $M_{H I}$

We examine the total C II luminosity of the $z \simeq 6$ simulated galaxies and its connection to the total diffuse H I gas mass in Figure 1, color coded as a function of SFR. In previous work, Vizgan et al. (2022) attempted to test and verify the use of C II as a tracer of the molecular gas based on the same set of simulated galaxies at $z \approx 6$. They found a sublinear relation between M_{mol} and $L_{[C\ II]}$, in contrast with the linear relation described by Zanella et al. (2018), which arose as a consequence of the Kennicutt–Schmidt law. By performing a log-linear fit to the data, we find a strong correlation between the C II and H I, yielding a best-fit relation of

$$\log L_{[C\ II]} = 1.02 \log M_{H\ I} - 1.95. \qquad (1)$$

with an rms scatter of 0.39 dex. For comparison, we examine the relation between $L_{[C\ II]}$ and M_{mol} and SFR within these simulations. We find that scatter is notably tighter than $L_{[C\ II]}$ versus M_{mol} (0.45 dex) and than $L_{[C\ II]}$ versus SFR (0.50 dex) for our simulations (Vizgan et al. 2022). This is further support of C II being most tightly connected to H I, and thus a more reliable tracer of this gas phase. Figure 2 of Vizgan et al. (2022) demonstrated that C II emission was most negligible from H I regions in these simulations; we highlight, though, that we want to calibrate the inferred H I mass with the total [C II] emission—irrespective of origin—as this is what we ultimately observe from the high-z galaxies.

3.2. The Metallicity Dependence of the [C II]-to-[H I] Conversion Factor

Defining the C II-to-H I conversion factor as $\beta_{[C\ II]} = M_{H\ I}/L_{[C\ II]}$ (Heintz et al. 2021), we derive a median
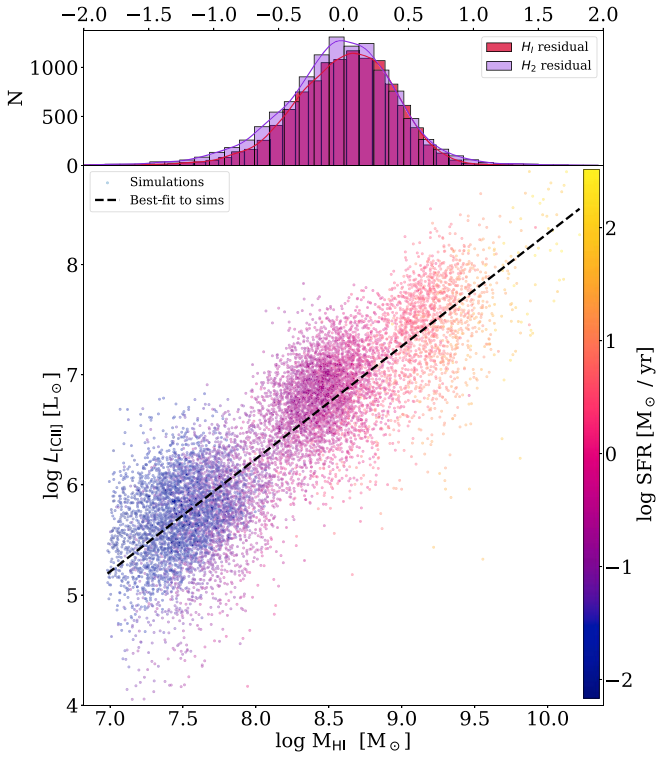
Figure 1. Top panel: histograms of scatter around the best-fit models for the C II-to-H I relation (this work, crimson) and for the C II–H₂ relation (Vizgan et al. 2022, violet); the scatter around the former relation is tighter (0.39 dex) than for the C II–H₂ relation (0.45 dex). Bottom figure: the C II luminosity vs. H I gas mass relation for our $z \simeq 6$ simulations. We find a very strong linear correlation between these two quantities, yielding a best-fit of $\log L_{[\mathrm{C\,II}]} = 1.02 \log M_{\mathrm{H\,I}} - 1.95$. The simulations are color coded by the star formation rate, further demonstrating a correlation between SFR and the log-linear C II–H I relation. When accounting only for the diffuse H I mass derived from CLOUDY, the relation changes to $\log L_{[\mathrm{C\,II}]} = 0.84 \log M_{\mathrm{H\,I}} + 0.55$ with a scatter of 0.22 dex.

$\log \beta_{[\mathrm{C\,II}]} = 1.7^{+0.4}_{-0.3} M_\odot / L_\odot$ for our set of simulated galaxies at $z \approx 6$. Heintz et al. (2021) determined that $\beta_{[\mathrm{C\,II}]} = M_{\mathrm{H\,I}}/L_{[\mathrm{C\,II}]}$ evolves with metallicity, following

$$\log M_{\mathrm{H\,I}}/L_{[\mathrm{C\,II}]} = (-0.87 \pm 0.09) \times \log(Z/Z_\odot) + (1.48 \pm 0.12). \quad (2)$$

This C II-to-H I relation is derived from a combination of high-z GRB afterglows, assuming that their pencil-beam sightlines probe representative regions of the star-forming ISM, and was found to show remarkable consistency with direct observations of local galaxies (Heintz et al. 2021).

In Figure 2 we examine the evolution of $\beta_{[\mathrm{C\,II}]}$ with metallicity within our simulations. For comparison, we over-plot the measurements at $z = 1.7$–6.3 from the GRB sightlines (Heintz et al. 2021) and the local set of observations (Cormier et al. 2015). We find an anticorrelation between $\beta_{[\mathrm{C\,II}]}$ and Z with our simulations (with r/Pearson coefficient = -0.20), in strong agreement with Heintz et al. (2021) and the local galaxy sample. Additionally, there appears to be a slight correlation between $\beta_{[\mathrm{C\,II}]}$ and star formation rate. The anticorrelation of $\beta_{[\mathrm{C\,II}]}$ is mostly a result of the definition; i.e., C II/H I is a proxy to carbon/hydrogen; hence, the galaxies that are more metal-rich will have more carbon available, both in the neutral and ionized states.
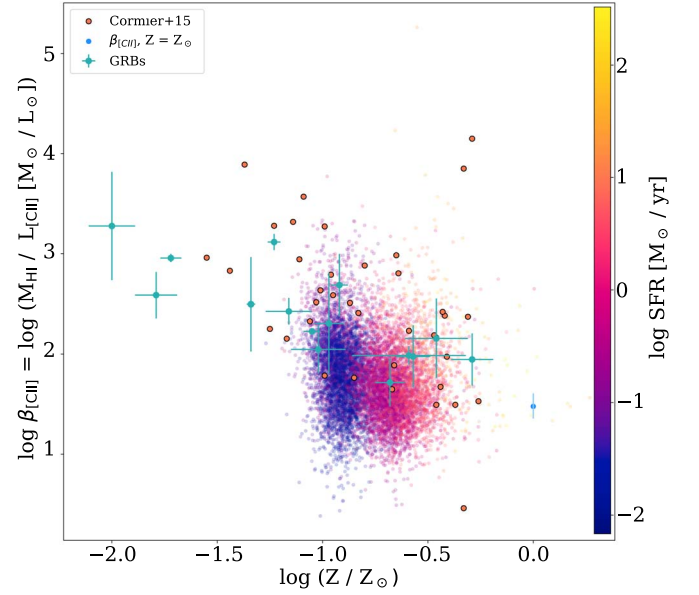

Figure 2. The [C II]-to-H I conversion factor $\beta_{[CII]}$ vs. SFR-weighted metallicity. The blue dot is $\beta_{[C\,II]} = 30^{+10}_{-7} M_\odot/L_\odot$, the conversion factor at solar metallicities (Heintz et al. 2021). GRBs are taken from Selsing et al. (2019; see also Heintz et al. 2021), while the orange points are the galaxies from Cormier et al. (2015).

4. The H I Gas Mass Budget of Galaxies at $z \approx 6$

With this set of simulations, we further make predictions of the H I gas mass fraction of galaxies at $z \approx 6$. Defining the H I gas mass excess as $M_{\mathrm{H\,I}}/M_\star$, we find a mean and median $M_{\mathrm{H\,I}}/M_\star = 1.4$ and $1.2^{+0.9}_{-0.6}$, respectively. We also predict the fraction of H I by mass to the total baryonic matter content $M_{\mathrm{bar,tot}} = M_{\mathrm{H\,I}} + M_{\mathrm{H_2}} + M_\star$. We find a mean and median fraction of $M_{\mathrm{H\,I}}/M_{\mathrm{bar,tot}} = 0.45$ and $0.46^{+0.12}_{-0.13}$, respectively. By comparison, the mean $M_{\mathrm{H_2}}/M_{\mathrm{bar,tot}}$ is 0.17 and median $0.15^{+0.10}_{-0.06}$; the mean $M_\star/M_{\mathrm{bar,tot}}$ is 0.38, and the median is $0.37^{+0.14}_{-0.11}$. We thus predict that H I is the dominant, baryonic matter component in galaxies at $z \approx 6$.

Several observational works (e.g., Zanella et al. 2018; Dessauges-Zavadsky et al. 2020) have investigated the use of C II as a molecular gas mass tracer. Vizgan et al. (2022) showed that the $\alpha_{[\mathrm{C\,II}]}$ derived by Zanella et al. (2018; Z18) required further calibration, as the slope of the log-linear [C II]-M_{mol} relation was not near unity. Dessauges-Zavadsky et al. (2020) used the Z18 $\alpha_{[\mathrm{C\,II}]}$ relation to derive the molecular gas budgets of their observations across redshift.

In Figure 3 we investigate the evolution of the H I gas mass budget, comparing the data from the ALPINE C II survey (e.g., Dessauges-Zavadsky et al. 2020) with our simulations. The H I gas masses in the ALPINE data are derived first by deriving metallicities from their SFRs and stellar masses via the high-redshift mass–metallicity relation in Curti et al. (2020), and then by using Equation (2) in this work (also see Heintz et al. 2021). We find that the ALPINE data are in reasonable agreement with the simulations; direct metallicity measurements from the ALMA sources, which were not available in the data, would allow for better constraints on the H I gas mass. Nonetheless, the ALPINE data are consistent with the prediction from simulations that the H I gas mass content should dominate the ISM at high redshift. As the ALPINE team used the work from Zanella et al. (2018) to derive molecular
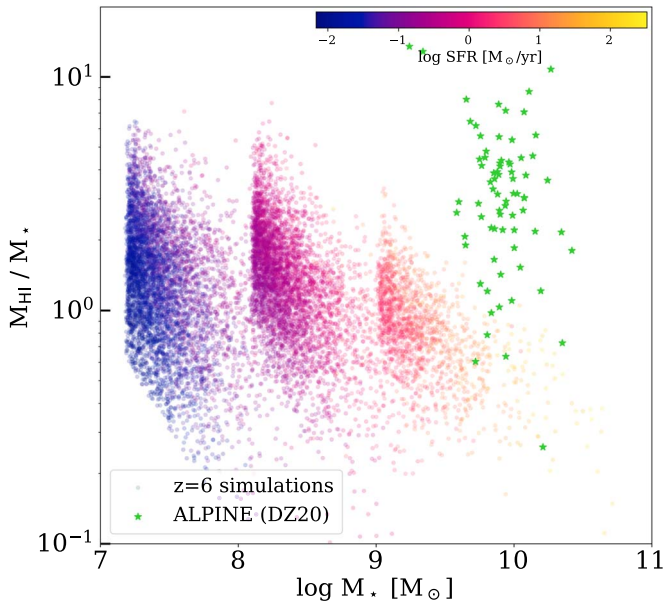
Figure 3. The evolution of the H I gas mass excess with stellar mass. Our simulations are color coded by star formation rate, and the y-axis is scaled logarithmically. The green stars represent galaxies from the ALPINE survey (Dessauges-Zavadsky et al. 2020). For the ALPINE data, we derive gas-phase metallicities from their $M_\star$ and SFRs using the mass–metallicity relation in Curti et al. (2020). From there, we use Equation (2) to derive estimates of their H I gas mass content.

gas masses for their sources, further work at high redshift should further examine the degree to which C II luminosity traces the H I, H$_2$, or both gas masses, as it appears to be a good tracer of both the neutral and molecular gas reservoirs that occupy the ISMs of high-redshift galaxies.

5. Conclusions

Previously, C II has been used as a tracer of SFR in galaxies (e.g., De Looze et al. 2014), and more recently as a tracer of H$_2$ gas mass (e.g., Zanella et al. 2018; Dessauges-Zavadsky et al. 2020; Madden et al. 2020; Vizgan et al. 2022). In this work, we use a set of simulated galaxies at $z \simeq 6$ (Vizgan et al. 2022) to investigate the utility of C II luminosity as a tracer of atomic (i.e., diffuse) hydrogen gas mass, following the work of Heintz et al. (2021). We present our main findings below:

1. For our SIMBA simulations at $z = 6$, we are able to find a strong relationship between C II luminosity and H I gas mass: $\log L_{[C II]} = 1.02 \log M_{H I} - 1.95$. Significantly, the relation is more tightly correlated (0.39 dex) than the C II-to-H$_2$ (0.45 dex) and C II-to-SFR (0.50 dex) correlations described in Vizgan et al. (2022). Furthermore, we find an anticorrelation of of $\beta_{[C II]}$ with metallicity.
2. We find that the H I gas mass is a critical baryonic matter component, with mean $M_{H I}/M_\star = 1.4$, and $M_{H I}/M_{\mathrm{bar,tot}} = 0.45$. We conclude that in the high-redshift universe, galaxies' ISMs (excluding dust) are dominated by H I baryonic matter content.
3. We compare our work with archival C II observational data, finding that extrapolating H I gas masses from high-redshift C II sources in the ALPINE C II survey yields an evolution of the H I gas mass budget over stellar mass, which agrees with predictions from simulations.

We ultimately conclude that C II is a viable proxy to infer the amount of H I in galaxies at $z \approx 6$. C II is readily available in the high-redshift universe for large surveys (e.g., the Large ALMA-ALPINE survey at $z \sim 4$–6; Béthermin et al. 2020; Dessauges-Zavadsky et al. 2020; Faisst et al. 2020; Le Fèvre et al. 2020, etc.; and REBELS at $z \sim 6$–8; e.g., Bouwens et al. 2021; Heintz et al. 2022). Establishing a proxy for H I is particularly important as even the next-generation radio facilities such as the Square Kilometre Array will only be able to detect and measure H I out to $z \approx 2$ and will not be able to probe the evolution of H I in the universe beyond cosmic noon.

ORCID iDs

David Vizgan https://orcid.org/0000-0001-7610-5544
Kasper E. Heintz https://orcid.org/0000-0002-9389-7413
Thomas R. Greve https://orcid.org/0000-0002-2554-1837
Desika Narayanan https://orcid.org/0000-0002-7064-4309
Romeel Davé https://orcid.org/0000-0003-2842-9434
Karen P. Olsen https://orcid.org/0000-0003-1250-5287
Gergö Popping https://orcid.org/0000-0003-1151-4659
Darach Watson https://orcid.org/0000-0002-4465-8264

References

Bera, A., Kanekar, N., Chengalur, J. N., & Bagla, J. S. 2019, ApJL, 882, L7
Béthermin, M., Fudamoto, Y., & Ginolfi, M. 2020, A&A, 643, A2
Bolatto, A. D., Wolfire, M., & Leroy, A. K. 2013, ARA&A, 51, 207
Bolmer, J., Ledoux, C., Wiseman, P., et al. 2019, A&A, 623, A43
Bouwens, R. J., Smit, R., Schouws, S., et al. 2022, ApJ, 931, 160
Burgh, E. B., France, K., & Jenkins, E. B. 2010, ApJ, 708, 334
Carilli, C. L., & Walter, F. 2013, ARA&A, 51, 105
Chowdhury, A., Kanekar, N., Chengalur, J. N., Sethi, S., & Dwarakanath, K. S. 2020, Natur, 586, 369
Chowdhury, A., Kanekar, N., Das, B., Dwarakanath, K. S., & Sethi, S. 2021, ApJL, 913, L24
Cormier, D., Madden, S. C., Lebouteiller, V., et al. 2015, A&A, 578, A53
Curti, M., Mannucci, F., Cresci, G., & Maiolino, R. 2020, MNRAS, 491, 944
Dave, R., Angles-Alcazar, D., Narayanan, D., et al. 2019, MNRAS, 486, 2827

De Looze, I., Cormier, D., Lebouteiller, V., et al. 2014, A&A, 568, A62
Dessauges-Zavadsky, M., Ginolfi, M., Pozzi, F., et al. 2020, A&A, 643, A5
Faisst, A. L., Schaerer, D., Lemaux, B. C., et al. 2020, ApJS, 247, 61
Fernandez, X., Gim, H. B., Gorkom, J. H. v., et al. 2016, ApJL, 824, L1
Heiles, C., & Troland, T. H. 2003, ApJ, 586, 1067
Heintz, K. E., Oesch, P. A., Aravena, M., et al. 2022, ApJL, 934, 27
Heintz, K. E., Watson, D., Oesch, P., Narayanan, D., & Madden, S. C. 2021, ApJ, 922, 147
Hollenbach, D. J., & Tielens, A. G. G. M. 1999, RvMP, 71, 173
Kalberla, P. M. W., Burton, W. B., Hartmann, D., et al. 2005, A&A, 440, 775
Le Fèvre, O., Béthermin, M., Faisst, A., et al. 2020, A&A, 643, A1
Leung, T. K. D., Olsen, K. P., Somerville, R. S., et al. 2020, ApJ, 905, 102
Lupi, A., & Bovino, S. 2020, MNRAS, 492, 2818
Madau, P., & Dickinson, M. 2014, ARA&A, 52, 415
Madden, S. C., Cormier, D., Hony, S., et al. 2020, A&A, 643, A141
Madden, S. C., Geis, N., Genzel, R., et al. 1993, ApJ, 407, 579
Madden, S. C., Poglitsch, A., Geis, N., Stacey, G. J., & Townes, C. H. 1997, ApJ, 483, 200
Madden, S. C., Remy-Ruyer, A., Galametz, M., et al. 2013, PASP, 125, 600
Morton, D. C., & Hu, E. M. 1975, ApJ, 202, 638
Olsen, K., Greve, T. R., Narayanan, D., et al. 2017, ApJ, 846, 105
Papadopoulos, P. P., & Greve, T. R. 2004, ApJL, 615, L29
Ramos Padilla, A. F., Wang, L., Ploeckinger, S., van der Tak, F. F. S., & Trager, S. C. 2021, A&A, 645, A133

Ramos Padilla, A. F., Wang, L., van der Tak, F. F. S., & Trager, S. 2022, arXiv:2205.11955
Scott, D., & Rees, M. J. 1990, MNRAS, 247, 510
Selsing, J., Malesani, D., Goldoni, P., et al. 2019, A&A, 623, A92
Stacey, G. J., Hailey-Dunsheath, S., Ferkinhoff, C., et al. 2010, ApJ, 724, 957
Swaters, R. A., van Albada, T. S., van der Hulst, J. M., & Sancisi, R. 2002, A&A, 390, 829
Taylor, M. B. 2005, in ASP Conf. Seri. 347, Astronomical Data Analysis Software and Systems XIV, ed. P. Shopbell, M. Britton, & R. Ebert (San Francisco, CA: ASP), 29
Thuan, T. X., & Martin, G. E. 1981, ApJ, 247, 823
Tielens, A. G. G. M., & Hollenbach, D. 1985, ApJ, 291, 722
Turk, M. J., Smith, B. D., Oishi, J. S., et al. 2011, ApJS, 192, 9
Vallini, L., Gallerani, S., Ferrara, A., Pallottini, A., & Yue, B. 2015, ApJ, 813, 36
Vizgan, D., Greve, T. R., Olsen, K. P., et al. 2022, ApJ, 929, 92
Walter, F., Brinks, E., de Blok, W. J. G., et al. 2008, AJ, 136, 2563
Wolfire, M. G., Hollenbach, D., McKee, C. F., Tielens, A. G. G. M., & Bakes, E. L. O. 1995, ApJ, 443, 152
Wolfire, M. G., McKee, C. F., Hollenbach, D., & Tielens, A. G. G. M. 2003, ApJ, 587, 278
Zanella, A., Daddi, E., Magdis, G., et al. 2018, MNRAS, 481, 1976